Check for updates

ChemCatChem

Research Article
doi.org/10.1002/cctc.202401462

Chemistry Europe
European Chemical Societies Publishing

www.chemcatchem.org

The Simultaneous Total Oxidation of Toluene, Propene, and CO Environmental Pollutants Using Bimetallic Au-Pt/ZrO_2/UVM-7 Catalysts

Kieran J. Aggett,[a] Tomás García,[b] David J. Morgan,[a] Mario Peláez-Fernández,[c, d] Álvaro Mayoral,[c, d] Raul Arenal,[c, d, e] Benjamín E. Solsona,[f] Pedro Amorós,[g] and Stuart H. Taylor*[a]

Supported precious metal catalysts, containing either mono or bimetallic Au and Pt nanoparticles, anchored on a hierarchical porous UVM-7 silica structure, were prepared and evaluated for the removal of volatile organic pollutants by oxidation. The catalysts were investigated for the simultaneous total oxidation of three model compounds: propene, toluene, and CO, commonly associated with "cold start pollutants" in automotive exhausts. Only Au showed low catalytic activity, while Pt nanoparticles were active, with a greater concentration of accessible Pt nanoparticles corresponding with increased catalytic activity. Interestingly, having both metals present on the same catalyst together was preferential for producing higher activity in the total oxidation of CO, propene, and toluene. The loadings of Pt nanoparticles on the catalyst surface, as well as the synthesis method, were important controlling factors. The order of metal loading deposition was influential, depositing Au and Pt sequentially resulted in surface enrichment of the latter deposited metal, leading to enhanced catalytic performance. When Au and Pt were loaded simultaneously, alloy formation occurred, and the surface Pt enrichment was more moderate, but still maintaining better catalytic performance compared with the pure Pt catalyst.

1. Introduction

Volatile organic compounds (VOCs) are a large category of the organic compounds emitted from natural or anthropogenic sources that enter the environment. Many studies have shown that anthropogenic VOCs are major contributors to air pollution, with the ability to react with NO_x species, forming photochemical smog, and as precursors to the formation of secondary aerosols.[1,2] Furthermore, VOCs promote adverse effects on human health and the environment.[3] The definition of a VOC is broad and encompasses a variety of compounds, with key examples being aliphatic and aromatic hydrocarbons. Automotive exhaust emissions and industrial processes are major sources of anthropogenic VOC emissions.[3,4] Regarding automotive exhaust emissions, a significant issue is the effect of cold start conditions. This can be defined by the engine and catalytic converter not yet operating at regular optimal temperature, resulting in higher rates of incomplete combustion.[5] These conditions can account for around 70% of emissions during vehicle testing and lead to greater VOC output due to exhaust catalysts not reaching light-off temperatures quick enough to remove the pollutants.[6,7] Of the prominent VOCs emitted from combustion engines, propene and toluene are of great concern due to their high photochemical ozone creativity potential (POCP).[8] Furthermore, aromatic VOCs, such as toluene and benzene, are also known to be highly toxic,[9] highlighting the importance of limiting VOC emissions. In addition to VOCs, carbon monoxide (CO) is also a common product emitted from combustion processes[10] and is known to be hazardous to human health under prolonged exposure.[11]

The utilization of VOC and CO mixtures is therefore an effective model when studying abatement methods of these emissions from vehicle exhausts. The removal of mixtures containing chemically varying compounds can prove challenging due to the

[a] Dr. K. J. Aggett, Dr. D. J. Morgan, Prof. S. H. Taylor
Cardiff Catalysis Institute, School of Chemistry, Cardiff University, Translational Research Hub, Maindy Road, Cardiff CF24 4HF, UK
E-mail: taylorsh@cardiff.ac.uk

[b] Dr. T. García
Instituto de Carboquimica (ICB-CSIC), C/Miguel Luesma Castán, Zaragoza 50018, Spain

[c] Dr. M. Peláez-Fernández, Dr. Á. Mayoral, Dr. R. Arenal
Instituto de Nanociencia y Materiales de Aragón (INMA), CSIC-Universidad de Zaragoza, Zaragoza 50009, Spain

[d] Dr. M. Peláez-Fernández, Dr. Á. Mayoral, Dr. R. Arenal
Laboratorio de Microscopias Avanzadas (LMA), Universidad de Zaragoza, Mariano Esquillor S/N, Zaragoza 50018, Spain

[e] Dr. R. Arenal
ARAID Foundation, Zaragoza 50018, Spain

[f] Prof. B. E. Solsona
Department of Chemical Engineering, University of Valencia, Av. Universitats s/n, Burjassot 46100, Spain

[g] Prof. P. Amorós
Institut de Ciéncia dels Materials (ICMUV), Universitat de València, Carrer del Catedrátic José Beltrán Martinez, 2, Paterna, València 46980, Spain

Supporting information for this article is available on the WWW under https://doi.org/10.1002/cctc.202401462

© 2025 The Author(s). ChemCatChem published by Wiley-VCH GmbH. This is an open access article under the terms of the Creative Commons Attribution License, which permits use, distribution and reproduction in any medium, provided the original work is properly cited.

© 2025 The Author(s). ChemCatChem published by Wiley-VCH GmbH

complex nature of the system. Recovery methods tend to be less effective approaches of abatement for these types of emission sources, owing to the relatively low concentrations of pollutants emitted.[12] In contrast, catalytic oxidation is recognized as an efficient method for controlling and removing low concentrations of pollutant mixtures. Catalytic oxidation has the advantage of being less energy intensive compared with standard thermal oxidation, while also producing more environmentally benign products by minimizing partial oxidation reactions.[13]

Supported precious metal catalysts are amongst the most effective catalysts for VOC oxidation.[14–18] Notably, supported Pt catalysts have been extensively studied for VOC total oxidation, presenting significant activity for aliphatic and aromatic hydrocarbons.[19–21] Alternatively, supported catalysts containing Au have shown considerable activity for CO oxidation.[19,22] More recently, studies have reported improved catalytic activity for total oxidation reactions when using bimetallic metal systems.[23–26] It is reported that bimetallic systems can manipulate factors such as metal particle size and distribution, improve stability, and form new active alloyed structures, which can enhance catalytic activity.[24,27–29] The use of mesoporous structures as supports for these catalysts can provide accessible pore networks for better diffusion of organic pollutants, as well as increase nanoparticle dispersion and improve catalyst stability due to confinement effects.[30] However, these interactions are sometimes not enough to inhibit particle agglomeration. The addition of metal oxide promoters has been shown to enhance the stability of nanoparticles from sintering, as discussed in previous literature.[31] Work prior to this publication screened different metal oxide supports over UVM-7 material and found ZrO_2 to be a suitable candidate. The addition of ZrO_2 to catalyst systems is well regarded for its ability to enhance thermal stability, with the most commonly known example being the three-way catalyst for VOC oxidation. As Pt-based catalysts are known to be efficient for VOC total oxidation, the enhancement of these catalysts by incorporating another metal onto the support is an important focus of this research area. Previous work from the authors has demonstrated Au nanoparticles, anchored on metal oxides, which are supported on a UVM-7 structure, were active and stable for the total oxidation of single pollutants: CO, propane, and toluene.[30,32,33] It is therefore postulated that synergistic effects between the addition of Pt nanoparticles to a similar system could produce highly active catalysts for the simultaneous removal of both VOCs and CO.

Directives such as EURO 7 and the Paris Agreement provide increasing regulation of vehicle emissions to reduce the number of pollutants emitted. With increased monitoring of pollutant concentrations, more practical assessment of catalytic abatement technology is required. Many studies use single organic compounds to model VOC abatement by catalytic oxidation. However, removing a combination of VOCs, with different chemical characteristics simultaneously, has grown in interest due to the correlation with real-world conditions.[34] It is shown in the literature that mixtures of different pollutants can inhibit the removal of VOCs at low temperatures,[35,36] requiring more active catalysts that are efficient at removing a combination of pollutants.

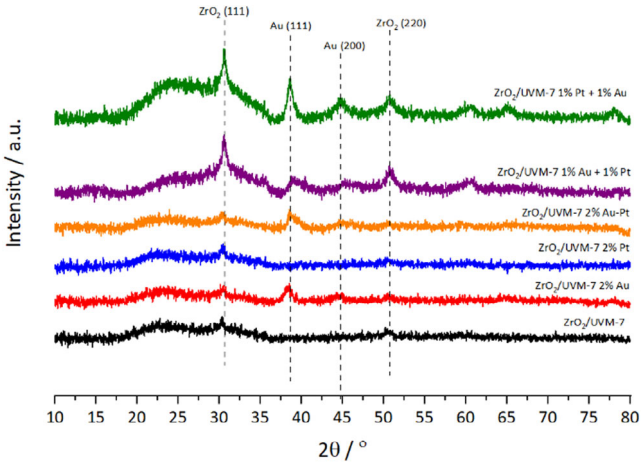

Figure 1. XRD patterns of the calcined catalysts.

In this work, a range of mono- and bimetallic-supported Pt–Au catalysts, prepared by colloidal deposition on the hierarchical porous UVM-7 silica support modified with ZrO_2, were evaluated for the simultaneous total oxidation of toluene, propene, and CO under oxygen-lean conditions. The gas mixture was used as an appropriate model to simulate cold start in vehicle engines, with propene and toluene VOCs used as a model for short-chain alkene and aromatic compounds, respectively.

2. Results and Discussion

2.1. Catalyst Characterization

An amorphous SiO_2 structure, expected from the UVM-7 support,[31] was predominantly shown in the XRD patterns of the catalysts (Figure 1). No reflections associated with Pt-containing crystalline phases were observed. Some crystalline tetragonal ZrO_2 species were identified, primarily around 30.3° and 50.0° (2θ), representing the (111) and (220) lattice planes, respectively.[37] Catalysts containing Au also exhibited a reflection around 38.9°, with a weaker reflection around 44.8°, which was ascribed to the Au (111) and (200) lattice planes, respectively.[38]

TPR analysis (Figure 2) displayed similar reduction profiles for each supported metal catalyst. The ZrO_2/UVM-7 catalyst presented two weak reduction peaks, one at high temperature around 615 °C and another broad low-temperature peak around 330 °C. These peaks can be attributed to the reduction of coordinatively unsaturated Zr^{4+} surface species and bulk Zr^{4+} species for the low-temperature and high-temperature peaks, respectively.[39] For the supported metal catalysts, two reduction peaks were also identified: an intense peak centered around 520 °C and a small broad peak centered around 200 °C. The presence of these peaks shifting upon the addition of Au or Pt metal nanoparticles to the support is in good agreement with previous literature,[40–42] where surface and bulk reduction of the Zr^{4+} species is enhanced by the supported metal nanoparticles.

© 2025 The Author(s). ChemCatChem published by Wiley-VCH GmbH

18673899, 0, Downloaded from https://chemistry-europe.onlinelibrary.wiley.com/doi/10.1002/cctc.202401462 by Welsh Assembly Government, Wiley Online Library on [13/03/2025]. See the Terms and Conditions (https://onlinelibrary.wiley.com/terms-and-conditions) on Wiley Online Library for rules of use; OA articles are governed by the applicable Creative Commons License

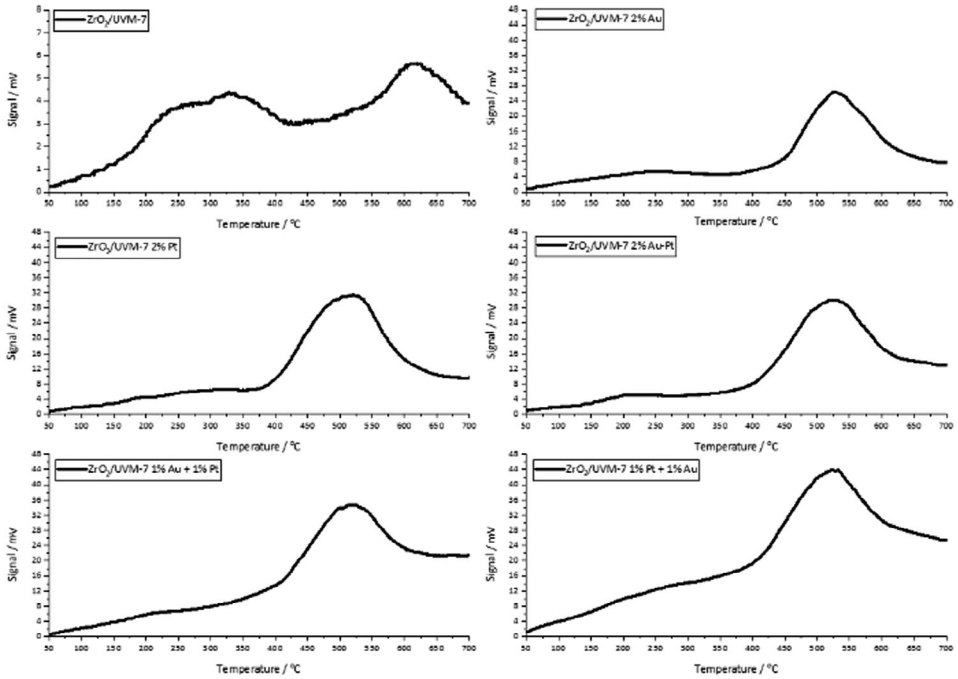

Figure 2. TRP profiles of the calcined catalysts.

Table 1. Summary of TPR data showing H_2 consumption per gram of catalyst for both high-temperature and low-temperature peaks.

Catalyst	Low Temperature Peak Position (°C)	High Temperature Peak Position (°C)	Low Temperature H_2 Consumption (μmol g^{-1})	High Temperature H_2 Consumption (μmol g^{-1})
ZrO_2/UVM-7	329	619	4.25	2.33
ZrO_2/UVM-7 2% Au	236	525	5.35	28.05
ZrO_2/UVM-7 2% Pt	200	520	2.43	38.83
ZrO_2/UVM-7 2% Au−Pt	205	517	2.29	33.91
ZrO_2/UVM-7 1% Au + 1% Pt	204	514	1.16	29.25
ZrO_2/UVM-7 1% Pt + 1% Au	207	522	2.02	38.28

Table 1 shows the H_2 consumption per catalyst mass for both the low-temperature and high-temperature reduction features of ZrO_2. The addition of metal nanoparticles to the ZrO_2/UVM-7 catalyst increased the H_2 consumption for the high-temperature peak, suggesting that the addition of the metal nanoparticles facilitated the reduction of bulk Zr^{4+} species. In contrast, only the ZrO_2/UVM-7 2% Au catalyst showed improved reduction of surface Zr^{4+} species, with all other catalysts presenting decreased H_2 consumption for the low-temperature reduction peak.

CO-DRIFTS analysis (Figure 3) was used to identify the types of metal nanoparticles present on the catalyst surface. Catalysts ZrO_2/UVM-7 2% Au−Pt and ZrO_2/UVM-7 1% Au + 1% Pt displayed a distinctive band at 2075 cm^{-1}. This band was attributed to CO linearly adsorbed on Pt surface sites, as suggested in previous literature.[43,44] It can be deduced from the presence of this band that both these catalysts had accessible Pt surface species, which could participate in the oxidation reaction. Moreover, the absence of this band from ZrO_2/UVM-7 2% Pt and ZrO_2/UVM-7 1% Pt + 1% Au implies limited Pt surface species available on the catalysts. Bands related to the adsorption of CO on Au species, expected between 2110 and 2176 cm^{-1},[45] were not present, possibly suggesting weak bonding due to limited available Au surface species.[46] A small residual band was identified at 1626 cm^{-1} for the support and monometallic catalysts,

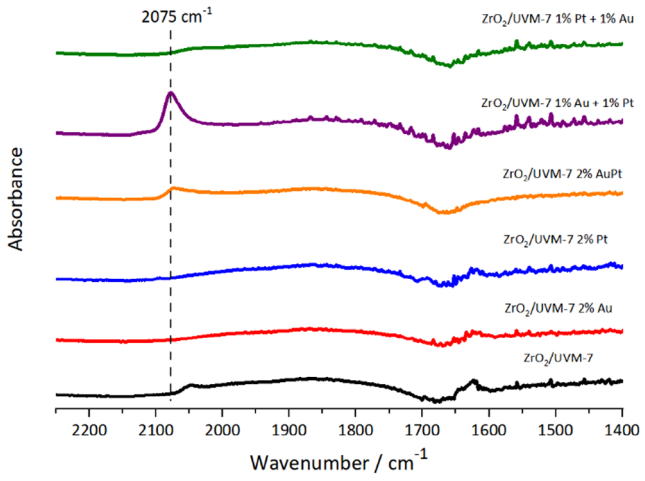

Figure 3. CO-DRIFTS spectra of the calcined catalysts.

© 2025 The Author(s). ChemCatChem published by Wiley-VCH GmbH

18673899, 0, Downloaded from https://chemistry-europe.onlinelibrary.wiley.com/doi/10.1002/cctc.202401462 by Welsh Assembly Government, Wiley Online Library on [13/03/2025]. See the Terms and Conditions (https://onlinelibrary.wiley.com/terms-and-conditions) on Wiley Online Library for rules of use; OA articles are governed by the applicable Creative Commons License

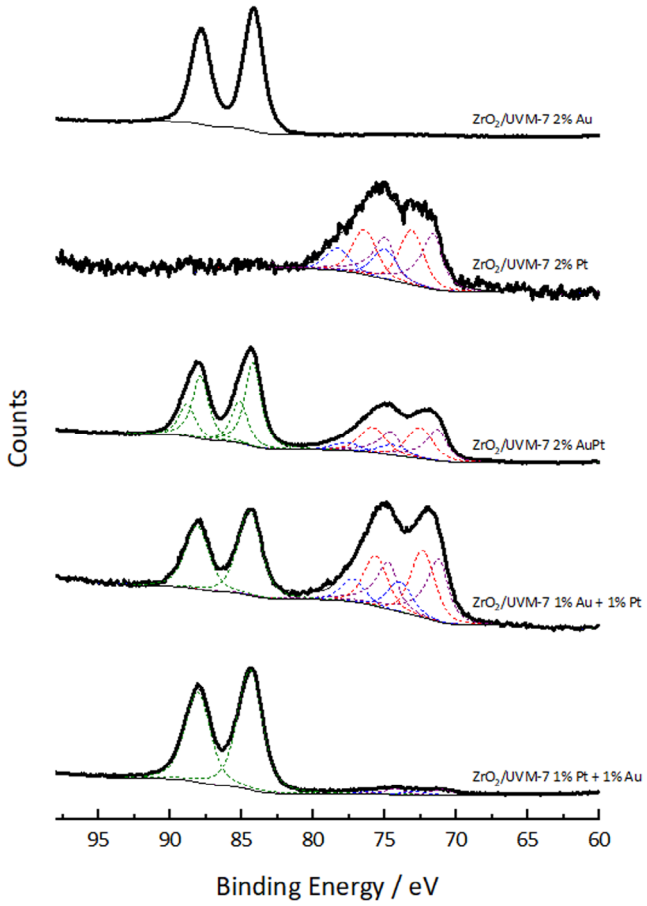

Figure 4. XPS spectra of the Au 4f and Pt 4f regions for the supported metal catalysts containing Au and Pt nanoparticles. Green curves represent the fitting of Au species. Purple, red, and blue curves represent the fitting of Pt^0, Pt^{II}, and Pt^{IV} species, respectively.

which has previously been linked to the formation of mono and bicarbonate species on the support surface.[47]

XPS analysis (Figure 4) was used to determine species on the catalyst surface. All Au-containing catalysts exhibited a metallic state indicated by the spin-orbit split peaks at 84.3 and 87.9 eV.[48] Further analysis of the Au peaks for the ZrO_2/UVM-7 2% Au−Pt catalyst revealed a Au species toward higher binding energy ($4f_{7/2}$ 85.2 eV) typical of Au^I.[49] Previous work has stated the presence of Au^I in AuPt/SiO_2 catalysts corresponded to interaction of the Pt and Au nanoparticles, by altering the electronic properties of the Au nanoparticles.[49] Therefore, a strong interaction of the Pt and Au nanoparticles for the ZrO_2/UVM-7 2% Au-Pt catalyst can be inferred, suggesting the possibility of alloy formation in this catalyst. However, it has been previously reported that Au species in this region can also be assigned as small Au nanoparticles or clusters.[50]

The Pt 4f region exhibits a broad structure for all Pt-containing catalysts. For the ZrO_2/UVM-7 2% Pt, ZrO_2/UVM-7 2% Au-Pt, and ZrO_2/UVM-7 1% Au + 1% Pt catalysts, the Pt spectral envelope could be fitted to Pt^0 (71.5 eV), Pt^{II} (73.1 eV), and Pt^{IV} (75 eV) species.[51,52] For the ZrO_2/UVM-7 1% Pt + 1% Au catalyst, the data could only be fitted to two Pt species: Pt^0 and Pt^{IV}. An observed shift to lower binding energies for the Pt species

Table 2. Surface species of Pt nanoparticles on Pt-containing catalysts, identified by XPS analysis.

Catalyst	Pt^0 (%)	Pt^{II} (%)	Pt^{IV} (%)
ZrO_2/UVM-7 2% Pt	42.3	37.9	19.8
ZrO_2/UVM-7 2% Au−Pt	42.7	42.8	14.5
ZrO_2/UVM-7 1% Au + 1% Pt	42.4	39.6	18.0
ZrO_2/UVM-7 1% Pt + 1% Au	67.9	–	32.1

was noticed in the bimetallic catalysts, with an average shift of −0.5 eV for ZrO_2/UVM-7 2% Au-Pt, −0.7 eV for ZrO_2/UVM-7 1% Au + 1% Pt, and −1.3 eV for ZrO_2/UVM-7 1% Pt + 1% Au. This shift to lower binding energies is proposed to occur as a result of the charge transfer from the interaction of Pt with Au nanoparticles, as shown in previous literature.[53,54] These data also suggest intimate contact of the different metal nanoparticles for the bimetallic catalysts, with stronger electron interaction implying the possibility of alloy formation.

Quantification of the Pt speciation (Table 2) indicated little difference in the relative concentrations of Pt species. Catalysts ZrO_2/UVM-7 2% Pt, ZrO_2/UVM-7 2% Au-Pt, and ZrO_2/UVM-7 1% Au + 1% Pt showed similar concentrations of metallic Pt^0 but had slight variations in Pt^{II} and Pt^{IV} concentrations. However, the ZrO_2/UVM-7 1% Pt + 1% Au catalyst showed considerable differences in Pt surface species, which was highlighted due to the absence of Pt^{II}, resulting in a much larger concentration of both Pt^0 and Pt^{IV} species.

All catalysts had a similar surface composition of Zr when analyzed by XPS, with concentrations ranging from 2 to 2.6 at.%, indicating strong interaction with the UVM-7 support (Table 3). However, the surface concentrations of supported metal nanoparticles varied for all catalysts. For the monometallic catalysts, increased surface loading of Au was identified for ZrO_2/UVM-7 2% Au, compared with the Pt loading on the ZrO_2/UVM-7 2% Pt catalyst. When analyzing the bimetallic catalysts, ZrO_2/UVM-7 2% Au-Pt displayed modest surface concentrations of both Pt and Au, with a near 1:1 ratio, which was in good agreement with the theoretical ratio expected. In contrast, this 1:1 surface ratio was not seen in the catalysts with differing orders of metal loading. The ZrO_2/UVM-7 1% Au + 1% Pt catalyst showed lower concentrations of surface Au and Pt; however, Pt enrichment was noted, with an Au–Pt ratio of 1:2, whereas the ZrO_2/UVM-7 1% Pt + 1% Au catalyst presented a 10:1 Au–Pt ratio, with a much higher surface concentration of Au.

These data demonstrate the importance of the order of metal loading on relative surface concentration. It is suggested that during sequential synthesis, the second metal is deposited preferentially on the first metal, resulting in a surface enrichment of the latter metal. Previous studies have shown that the preparation of bimetallic catalysts with a different metal deposition order exhibited little difference in the surface elemental composition, which is in contrast to the XPS data shown in this work.[23,55] However, this could be a result of the different preparation methods used. Colloidal deposition methods disconnect nanoparticle formation from the deposition step,

© 2025 The Author(s). ChemCatChem published by Wiley-VCH GmbH

18673899, 0, Downloaded from https://chemistry-europe.onlinelibrary.wiley.com/doi/10.1002/cctc.202401462 by Welsh Assembly Government, Wiley Online Library on [13/03/2025]. See the Terms and Conditions (https://onlinelibrary.wiley.com/terms-and-conditions) on Wiley Online Library for rules of use; OA articles are governed by the applicable Creative Commons License

Table 3. Catalyst surface composition, determined by XPS analysis.

Catalyst	Zr (at.%)	Pt (at.%)	Au (at.%)	Si (at.%)	O (at.%)	C (at.%)
ZrO_2/UVM-7	2.0	–	–	30.8	62.7	4.5
ZrO_2/UVM-7 2% Au	2.6	–	1.0	28.1	62.0	6.3
ZrO_2/UVM-7 2% Pt	2.2	0.1	–	29.4	61.5	6.8
ZrO_2/UVM-7 2% Au−Pt	2.2	0.7	0.7	26.5	58.8	11.0
ZrO_2/UVM-7 1% Au + 1% Pt	2.4	0.5	0.2	28.6	61.6	6.7
ZrO_2/UVM-7 1% Pt + 1% Au	2.4	0.1	0.9	28.2	61.7	6.7

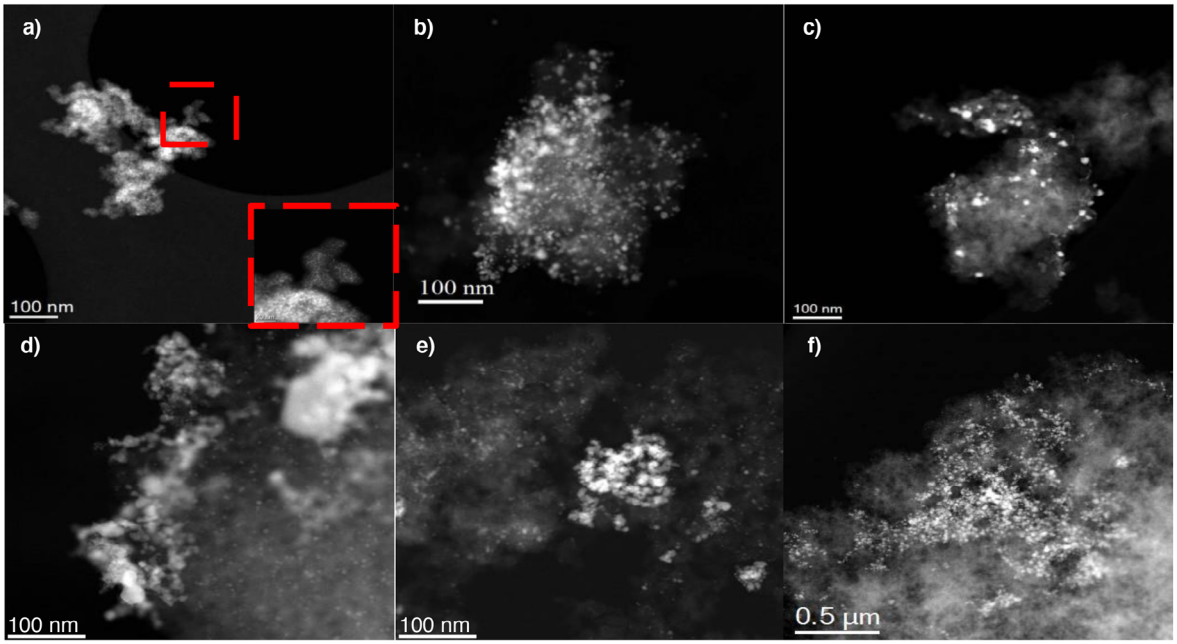

Figure 5. Low magnification Cs-corrected STEM-HAADF images of the calcined catalysts: (a) ZrO_2/UVM-7, (b) ZrO_2/UVM-7 2% Au, (c) ZrO_2/UVM-7 2% Pt, (d) ZrO_2/UVM-7 2% Au-Pt, (e) ZrO_2/UVM-7 1% Au + 1% Pt, and (f) ZrO_2/UVM-7 1% Pt + 1% Au.

carefully controlling influences of nanoparticle dispersion and particle size when preparing supported metal catalysts.[56] The use of this method in the current work emphasizes the order of metal loading as an influential factor for the XPS surface concentrations identified. Cs-corrected STEM-HAADF images (Figure 5f) indicated heterogeneously distributed Au and Pt metal nanoparticles on the ZrO_2/UVM-7 material for all the catalysts. However, a homogeneous distribution of ZrO_2 was observed by EDX analysis for all the catalysts, which is in good agreement with conclusions drawn from XPS analysis. Both EDX and XPS techniques suggest a strong interaction between the ZrO_2 and UVM-7 material, which could suggest confinement of the ZrO_2 as shown previously for TiO_2.[32] Cs-corrected STEM-EDX analysis identified Au and Pt nanoparticles for each of the monometallic catalysts, respectively.

The ZrO_2/UVM-7 2% Au catalyst (Figure 6a) had a large quantity of Au nanoparticles, with a size distribution between 2 and 10 nm and a mean particle size of 4.7 nm ± 1.6 nm. More Pt nanoparticles were identified on the ZrO_2/UVM-7 2% Pt catalyst, compared with Au nanoparticles on the monometallic Au catalyst, which was in contrast with the surface composition identified by XPS analysis. Furthermore, both small and larger clusters of Pt nanoparticles were identified (Figure 6b), resulting in a broader particle size distribution (2–20 nm), with a mean particle size of 6.0 nm ± 5.7 nm. The slight difference in the surface and bulk nanoparticles identified by both XPS and EDX could suggest migration to the internal porosity of the UVM-7 structure, as very large particles were not identified. It can also be seen from the EDX images in Figure 6 that Au and Pt nanoparticles were preferentially bound to the ZrO_2 support.

Both Au and Pt nanoparticles were identified by Cs-corrected STEM-EDX analysis for all bimetallic catalysts. The bimetallic catalysts showed co-located Au and Pt (Figure 7a–c), which suggests strong Au-Pt nanoparticle interaction. This was self-consistent with conclusions drawn from XPS analysis, suggesting the strong metal nanoparticle interaction resulted in the Pt species shifting to lower binding energies. Alloyed metal nanoparticles were observed in the ZrO_2/UVM-7 2% Au-Pt catalyst, with a large size distribution range of 3–100 nm and a mean particle size of 6.5 nm ± 6 nm. The presence of alloy formation may help to explain the appearance of Au^I species in the XPS data, reinforcing the suggestion of a strong electronic interac-

© 2025 The Author(s). ChemCatChem published by Wiley-VCH GmbH

18673899, 0, Downloaded from https://chemistry-europe.onlinelibrary.wiley.com/doi/10.1002/cctc.202401462 by Welsh Assembly Government, Wiley Online Library on [13/03/2025]. See the Terms and Conditions (https://onlinelibrary.wiley.com/terms-and-conditions) on Wiley Online Library for rules of use; OA articles are governed by the applicable Creative Commons License

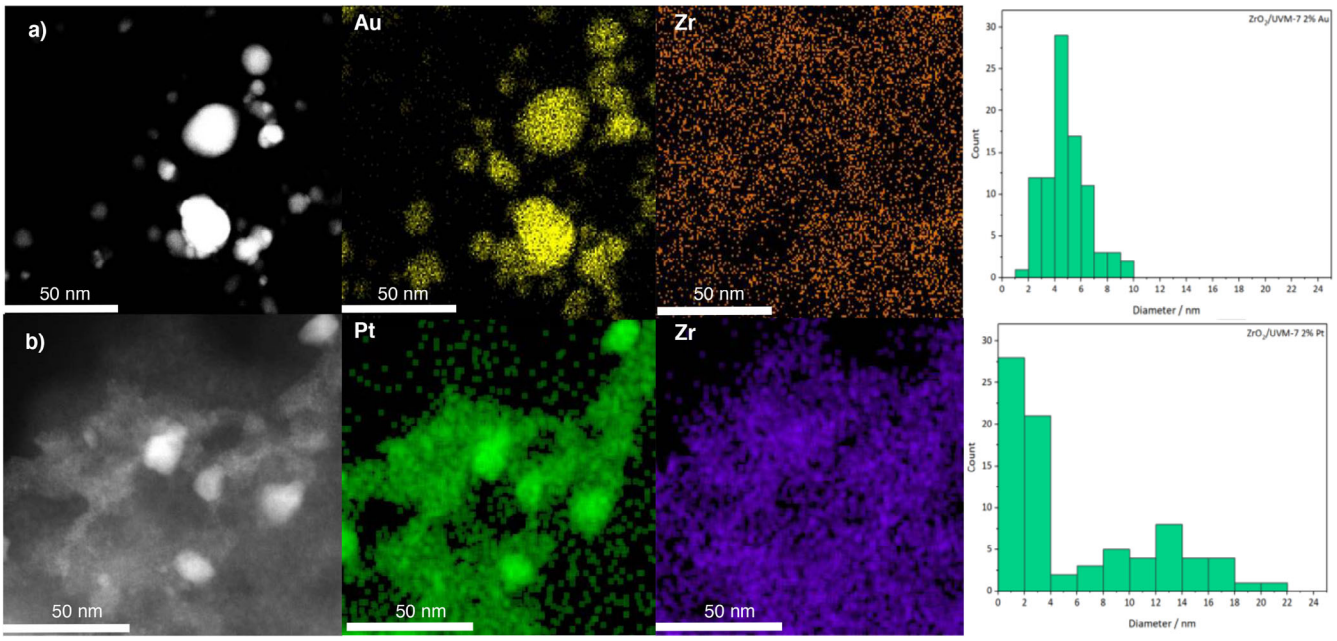

Figure 6. Cs-corrected STEM-HAADF with corresponding EDX images and particle size histograms of (a) ZrO_2/UVM-7 2% Au and (b) ZrO_2/UVM-7 2% Pt catalysts.

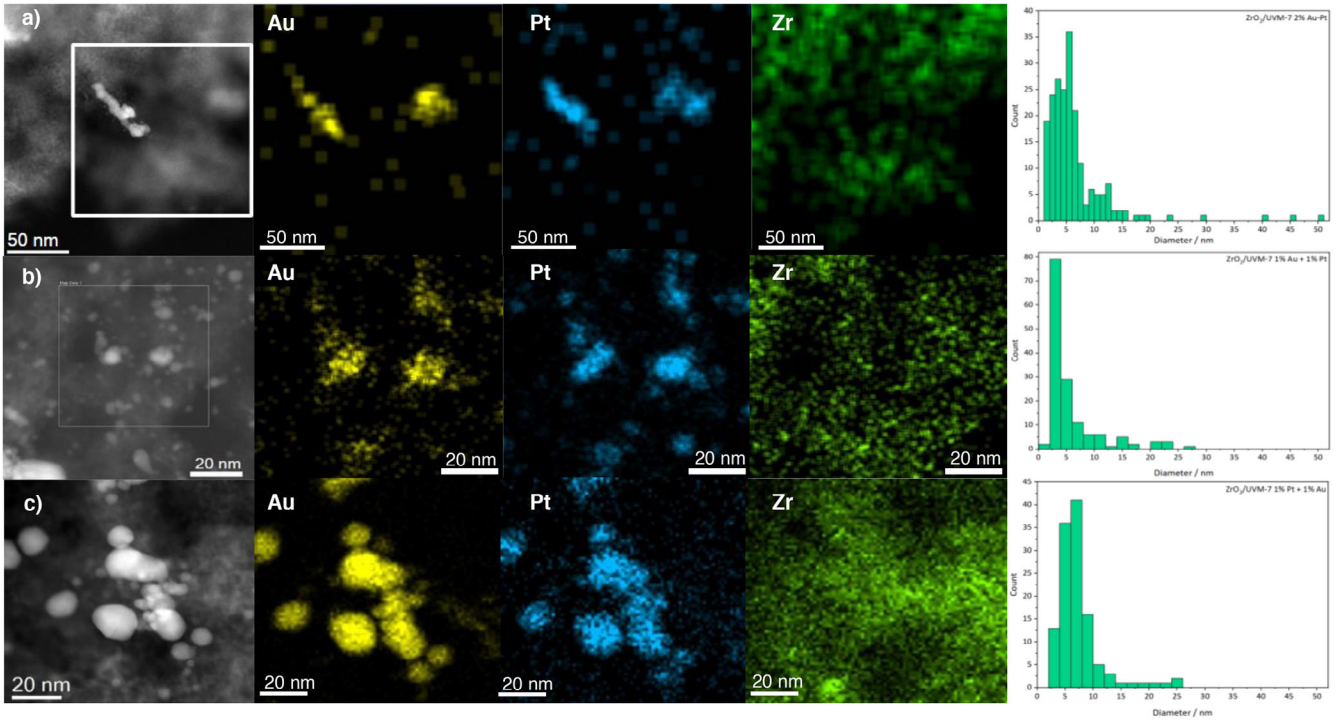

Figure 7. Cs-corrected STEM-HAADF images with corresponding EDX images and particle size histograms for the bimetallic catalyst: (a) ZrO_2/UVM-7 2% Au-Pt, (b) ZrO_2/UVM-7 1% Au + 1% Pt, and (c) ZrO_2/UVM-7 1% Pt + 1% Au.

tion of the Au-Pt species identified for this catalyst. It is also unlikely the shift in binding energy for the Au species in the XPS data was related to nanoparticle size, as little difference in average particle size is observed for the bimetallic catalysts. A heterogeneous particle size distribution was observed for the ZrO_2/UVM-7 1% Au + 1% Pt catalyst, with a mean particle size of 5.9 nm ± 5 nm. Both Au and Pt nanoparticles of >10 nm were formed; however, smaller nanoparticles (<5 nm), which were Pt rich, were also identified. The particle size distribution of the ZrO_2/UVM-7 1% Pt + 1% Au catalyst was comparable to the ZrO_2/UVM-7 1% Au + 1% Pt catalyst, but the smaller nanoparticles (<5 nm) were Au rich, and the mean particle size was slightly larger at 7.3 nm ± 4.1 nm. There was little significant difference in the average metal nanoparti-

© 2025 The Author(s). ChemCatChem published by Wiley-VCH GmbH

18673899, 0, Downloaded from https://chemistry-europe.onlinelibrary.wiley.com/doi/10.1002/cctc.202401462 by Welsh Assembly Government, Wiley Online Library on [13/03/2025]. See the Terms and Conditions (https://onlinelibrary.wiley.com/terms-and-conditions) on Wiley Online Library for rules of use; OA articles are governed by the applicable Creative Commons License

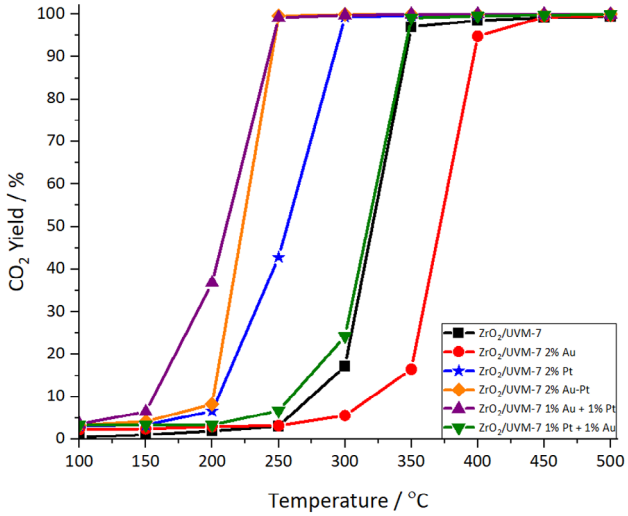

Figure 8. CO_2 yield acquired for the simultaneous total oxidation of toluene, propene, and CO gas mix. Conditions: 100 ppm toluene, 1000 ppm propene, 1000 ppm CO, 6% O_2/N_2, WHSV = 60,000 mL g^{-1} h^{-1}. Legend refers to catalysts used.

cle size across the range of catalysts, which was expected for the colloidal preparation method employed. The size distribution was larger for the bimetallic catalysts; however, this is likely to occur from the possible agglomeration of nanoparticles during the two-stage calcination process for the sequential preparation method and the formation of alloy nanoparticles for the simultaneous preparation method.

2.2. Catalyst Testing

Catalytic performance for the simultaneous total oxidation of propene, toluene, and CO is displayed in Figure 8 for all catalysts. CO_2 yield from the mixture was used to assess the overall catalytic activity for the combined total oxidation. The only product identified by FTIR analysis was CO_2, with all catalysts obtaining a carbon balance of >94% and in the 98%–102% range at conversions higher than 15%. The ZrO_2/UVM-7 1% Au + 1% Pt catalyst presented the highest catalytic activity, with all reactant compounds oxidized at 250 °C. Appreciable catalytic activity was also identified for the ZrO_2/UVM-7 2% Au-Pt catalyst, also reaching full conversion at 250 °C. However, this catalyst showed a lower CO_2 yield at temperatures under 250 °C, which could inhibit effectiveness when considering the application for emissions during the cold start period. The catalytic activity for the ZrO_2/UVM-7 2% Au catalyst was of particular interest, as the addition of Au to the support resulted in poorer activity when compared to the ZrO_2/UVM-7 support material.

The total oxidation of individual components in the gas mix are shown in Figure 9. The general trend of catalyst activity for each component is similar to the overall CO_2 yield presented, with the ZrO_2/UVM-7 1% Au + 1% Pt catalyst being the most active for all compounds. Only a slight deviation from the trend was observed for the oxidation of CO and toluene, where the ZrO_2/UVM-7 2% Au catalyst showed slightly improved conversion at low temperatures for CO oxidation, and the ZrO_2/UVM-7 1% Pt + 1% Au catalyst presented lower conversion than the support at 300 °C for toluene oxidation.

Previous literature has shown that the addition of a metal oxide onto a nonreducible support, such as Al_2O_3 or SiO_2, can improve the catalytic activity of supported metal catalysts for CO and VOC oxidation.[15,57,58] The metal oxide provides the beneficial role of supplying active oxygen species on the catalyst surface, which then enhances catalytic activity of the metal nanoparticles.[59,60] The promotion of active oxygen species has often been linked with surface reducibility of the catalyst, relating to the facile mobility of oxygen species.[58,61,62] In this work, no significant trend was distinguished between catalyst surface reducibility and catalytic activity. In fact, TPR analysis showed that the ZrO_2/UVM-7 2% Au catalyst, with the highest surface H_2 consumption, was the least active catalyst, implying other factors were important for controlling the activity. Therefore, the influence of metal nanoparticle loading had the largest impact on the overall catalytic activity.

The role of metal nanoparticles in supported precious metal catalysts is widely reported as an important factor for VOC and CO oxidation.[26,34,63,64] From the testing data in this work (Figure 8), catalysts containing high concentrations of Au nanoparticles, determined by XPS, showed poorer catalytic activity. Similar conclusions have been reported in previous studies

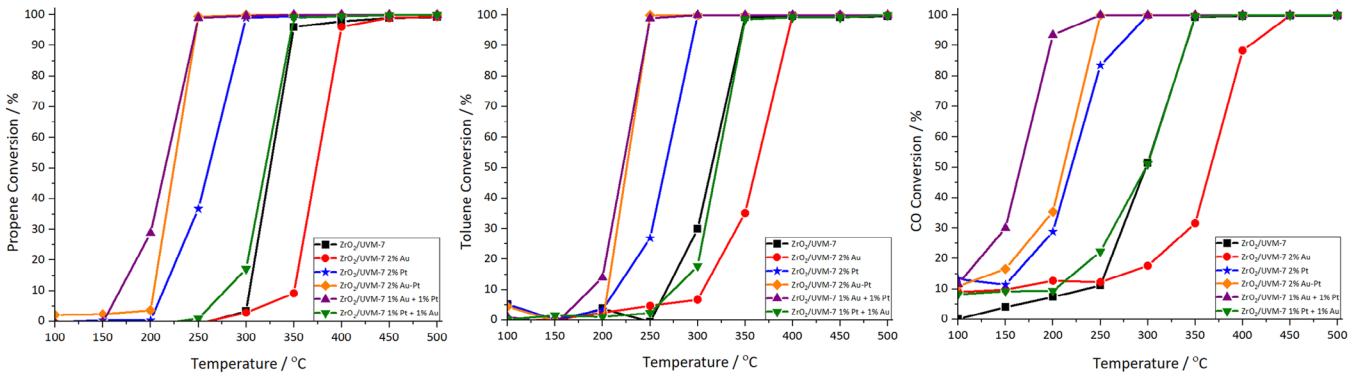

Figure 9. Breakdown of the catalytic activity for the total oxidation of individual pollutants in the mixed gas feed: propene (left), toluene (middle), and CO (right). Conditions: 100 ppm toluene, 1000 ppm propene, 1000 ppm CO, 6% O_2/N_2, WHSV = 60,000 mL g^{-1} h^{-1}.

© 2025 The Author(s). ChemCatChem published by Wiley-VCH GmbH

18673899, 0, Downloaded from https://chemistry-europe.onlinelibrary.wiley.com/doi/10.1002/cctc.202401462 by Welsh Assembly Government, Wiley Online Library on [13/03/2025]. See the Terms and Conditions (https://onlinelibrary.wiley.com/terms-and-conditions) on Wiley Online Library for rules of use; OA articles are governed by the applicable Creative Commons License

for the individual total oxidation of toluene and propene, where supported Au catalysts presented lower VOC conversion compared with Pt or Pd counterparts.[14,42,65] The lower catalytic activity was proposed to occur as a result of the differing intrinsic dissociative chemisorption energies of oxygen, which is related to the role of oxygen adsorption in the oxidation mechanism.[19] However, supported Au catalysts have been reported as effective catalysts for CO oxidation.[66,67] The prevalence for effective CO oxidation is presented by the ZrO_2/UVM-7 2% Au catalyst, as it showed improved performance at low temperatures (Figure 9). Previous literature discussing the simultaneous removal of VOCs and CO highlighted that VOCs competitively bind to the catalyst surface, blocking active sites and negatively impacting the rate of CO oxidation.[34,68] Therefore, the efficiency of supported Au catalysts for CO oxidation was decreased under the reaction conditions used.

From the previous discussion, it can be inferred that Pt was the most active species for the simultaneous total oxidation of CO, propene, and toluene. This hypothesis also fits well with surface compositions determined by XPS analysis when related to the catalytic activity. A structure-sensitive relationship has been determined for toluene and propene oxidation using supported Pt catalysts.[19,20,69,70] It has been shown that increased Pt particle size results in adsorbed oxygen on Pt with a lower bond strength, facilitating improved catalytic activity for toluene oxidation.[71] This differs from propene oxidation, where this affect is slightly less direct and can also be somewhat related to higher concentrations of metallic Pt^0 species.[69] Little significant difference in nanoparticle size was determined by Cs-corrected STEM-EDX analysis, suggesting this factor did not play an important role in determining the catalytic activity.

Little direct correlation between catalytic activity and the types of Pt surface species could be identified for these catalysts. There was a negligible difference in Pt^0 concentration and little significant difference in Pt^{II} and Pt^{IV} concentrations for the most active catalysts from the XPS data. Furthermore, a structure-sensitive relationship was not exhibited by these catalysts, as the ZrO_2/UVM-7 1% Au + 1% Pt catalyst contained a higher quantity of smaller Pt nanoparticles (<5 nm), determined by STEM analysis, compared with the ZrO_2/UVM-7 2% Pt catalyst, which showed lower catalytic activity. Therefore, the controlling factor determining catalytic activity was suggested to be the relative concentration of Pt on the catalyst surface, in comparison to the quantity of the less active Au nanoparticles. This trend is highlighted in Figure 10 by the direct correlation between decreasing temperature required to obtain 50% conversion (T_{50}) and increasing relative Pt concentration. CO-DRIFTS analysis further highlights the importance of surface Pt species, as the data indicated accessible surface Pt species for the ZrO_2/UVM-7 2% Au-Pt and ZrO_2/UVM-7 1% Au + 1% Pt catalysts only, which were concurrent with the improved activity of these catalysts. In contrast, an absence of Pt bands was displayed for the ZrO_2/UVM-7 2% Pt catalyst, possibly as a result of the low surface Pt loading, measured by XPS analysis.

The ZrO_2/UVM-7 2% Au-Pt and ZrO_2/UVM-7 1% Au + 1% Pt catalysts, with higher surface Pt concentrations, presented higher activity than the monometallic Pt catalyst. The improved performance of these bimetallic catalysts implies the addition of Au into the preparation method enhanced surface loading of Pt nanoparticles. Previous literature has suggested that Pt surface enrichment can occur in AuPt systems, due to the stronger affinity for adsorbates, forming stable oxides on the surface.[72] XPS data correlates well with this idea, as the ZrO_2/UVM-7 1% Pt + 1% Au catalyst presented a larger quantity of Pt^0 species, with less stable Pt oxide species formed, resulting in little surface migration.

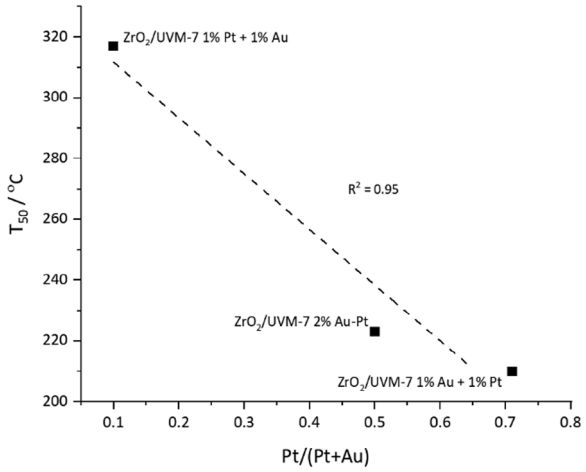

Figure 10. Relative Pt surface concentrations, identified by XPS analysis, compared with T_{50} values for the bimetallic Au-Pt catalysts.

The order of metal loading also significantly affected Pt loading on the catalyst surface. Depositing the metals sequentially caused a drastic change in catalytic activity, predominantly as a result of the improved surface concentration of Pt when it was deposited last (ZrO_2/UVM-7 1% Au + 1% Pt). However, depositing Au and Pt simultaneously led to both metal nanoparticles being evenly distributed on the surface, as demonstrated by the formation of alloyed nanoparticles in the Cs-corrected STEM-EDX analyses. The formation of alloyed nanoparticles resulted in a 1:1 surface ratio of Au-Pt, which led to slightly lower activity compared with the Pt rich 1:2 Au-Pt surface ratio obtained for the ZrO_2/UVM-7 1% Au + 1% Pt catalyst. This further highlights the negative impact caused by the increased amount of less active Au nanoparticles for the simultaneous oxidation of CO, propene, and toluene in this system.

The catalysts discussed in this work show promise as effective catalysts for low-temperature simultaneous oxidation of VOCs and CO. Specifically, the ZrO2/UVM-7 1% Au + 1% Pt catalyst showed key improvements from previous work by the authors for the total oxidation of toluene (Table 4). The ZrO2/UVM-7 1% Au + 1% Pt catalyst displayed a lower T50 compared with the Au/Co-UVM-7 catalyst, with the current work including the influence of other VOCs in the gas feed. It is difficult to directly compare the catalysts in this work with those shown in Table 4, due to the varying reaction conditions used. However, the catalysts in this work exhibited comparable, if not improved, T50 values with most of those displayed in Table 4 Furthermore, the conditions in the present work are generally closer to those applicable to automotive emissions, where oxygen concentrations are between 5%

© 2025 The Author(s). ChemCatChem published by Wiley-VCH GmbH

18673899, 0, Downloaded from https://chemistry-europe.onlinelibrary.wiley.com/doi/10.1002/cctc.202401462 by Welsh Assembly Government, Wiley Online Library on [13/03/2025]. See the Terms and Conditions (https://onlinelibrary.wiley.com/terms-and-conditions) on Wiley Online Library for rules of use; OA articles are governed by the applicable Creative Commons License

Table 4. Comparison of the total oxidation of VOC mixtures reported in the literature.

Catalyst	WHSV	Reaction Conditions	T_{50}[a] (°C)	Reference
ZrO_2/UVM-7 1% Au + 1% Pt	60,000 mL g^{-1} h^{-1}	1000 ppm propene, 1000 ppm CO, 100 ppm toluene, 6% O_2	215 (propene), 221 (toluene), 166 (CO)	This work
Au/Co-UVM-7	40,000 mL g^{-1} h^{-1}	1000 ppm toluene, 20% O_2	255	Previous work [30]
3% Au/CeO_2	25,000 mL g^{-1} h^{-1}	1000 ppm propene, 1000 ppm CO, 100 ppm toluene, 6% O_2	210 (propene), 160 (toluene), 119 (CO)	[73]
Pt-Co/Al_2O_3	60,000 mL g^{-1} h^{-1}	10,000 ppm CO, 1000 ppm toluene, 20% O_2	168 (CO), 182 (toluene)	[34]
Pt/CeO_2	60,000 mL g^{-1} h^{-1}	10,000 ppm CO, 1000 ppm toluene, 20% O_2	174 (CO), 180 (toluene)	[36]
CoAlCeO	60,000 mL g^{-1} h^{-1}	1000 ppm toluene, 1000 ppm CO, 20% O_2	248 (toluene)	[74]
Pd(shell)-Au(core)/TiO_2	60,000 mL g^{-1} h^{-1}	1000 ppm toluene, 3000 ppm propene, 20% O_2	~225 (toluene), ~230 (propene)	[23]
Mn_3O_4	30,000 mL g−1 h−1	1000 ppm VOCs (ethylene, propylene, toluene), 20% O_2	231 (conversion to CO_2)	[75]

a) *T50*: Temperature at which 50% conversion is obtained.

and 10%.[76] It should be highlighted that the "mixture effect," where multiple pollutants are present in a gas stream, has limited understanding of the inhibitor and promotional effects for different combinations of VOCs.[77] Therefore, further research is required in this area to provide clarity for different systems.

Interestingly, the work published on the 3% Au/CeO_2 catalyst by Eaimsumang et al.[73] presented slightly improved T_{50} values compared with the ZrO_2/UVM-7 1% Au + 1% Pt catalyst; however, a much lower WHSV was used. The contrast in activity for Au between the two studies shows the importance of the support. Additionally, CeO_2 is active for the total oxidation of toluene,[78,79] which will contribute to the efficient oxidation of this compound in the mixture. However, a significant limitation of CeO_2-based materials is the poor thermal stability, making them susceptible to sintering and deactivation.[80]

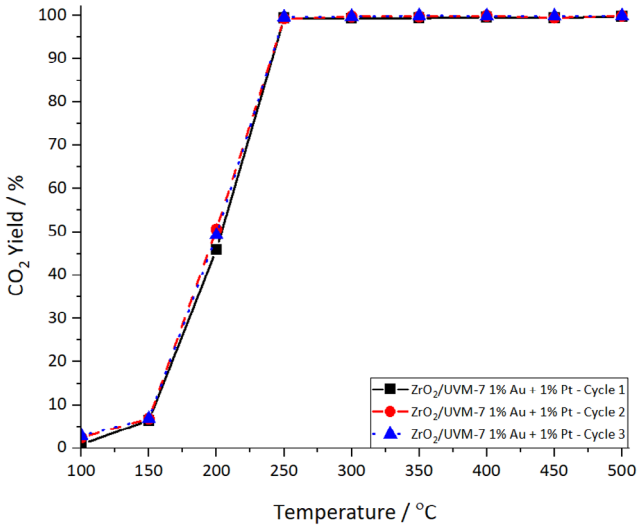

Figure 11. Consecutive cycle tests for the simultaneous total oxidation of toluene, propene, and CO using the ZrO_2/UVM-7 1% Au + 1% Pt catalyst. Conditions: 100 ppm toluene, 1000 ppm propene, 1000 ppm CO, 6% O_2/N_2, WHSV = 60,000 mL g^{-1} h^{-1}. Legend refers to the catalyst cycle.

2.3. Catalyst Stability

Catalyst stability is an important factor that needs to be considered. Previously, modified UVM-7 catalysts have displayed good thermal stability towards Au sintering. This was a result of the confinement architecture of the silica structure and strong anchoring onto the supported metal oxides that were homogeneously dispersed within the structure.[81] Catalytic cycle tests were carried out on the most active catalyst to assess the stability. The ZrO_2/UVM-7 1% Au + 1% Pt catalyst remained active with consistent performance for the total oxidation of toluene, propene, and CO after three consecutive cycles (Figure 11). This cyclic stability was also observed when the temperature was increased up to higher temperatures (600 °C or even 700 °C) for 10 min.

The considerable stability of this material highlights the UVM-7 structure as a suitable candidate for further modification when designing effective catalysts for the simultaneous total oxidation of VOCs and CO.

3. Conclusion

Mono and bimetallic Au-Pt catalysts, prepared using a novel ZrO_2/UVM-7 support, were assessed for the simultaneous total oxidation of toluene, propene, and CO under oxygen lean conditions. The gas mixture was used as a model as it represents significant emissions present during cold starts in automotive engines. The ZrO_2/UVM-7 1% Au + 1% Pt catalyst, in which Au is first deposited and then Pt, was the most active for the simultaneous total oxidation of all three compounds, attaining full conversion by 250 °C. The enhanced activity of this catalyst corresponded with the high relative surface concentration of Pt nanoparticles, which were identified as the active component for the reaction. For the bimetallic catalysts, the order of metal

© 2025 The Author(s). ChemCatChem published by Wiley-VCH GmbH

18673899, 0, Downloaded from https://chemistry-europe.onlinelibrary.wiley.com/doi/10.1002/cctc.202401462 by Welsh Assembly Government, Wiley Online Library on [13/03/2025]. See the Terms and Conditions (https://onlinelibrary.wiley.com/terms-and-conditions) on Wiley Online Library for rules of use; OA articles are governed by the applicable Creative Commons License

nanoparticle deposition was an important factor for controlling catalytic activity. Sequential loading of Pt and Au nanoparticles resulted in higher surface concentrations of active Pt nanoparticles and less active Au nanoparticles on the catalyst surface. In contrast, simultaneous addition of the metal nanoparticles formed alloyed nanoparticles with a 1:1 ratio on the catalyst surface. The alloyed nanoparticles displayed slightly lower catalytic activity, likely due to the increased surface concentration of Au. Finally, the optimal catalyst was demonstrated to be completely stable in the simultaneous CO, propene, and toluene removal after three catalytic cycles.

4. Experimental Section

4.1. Catalyst Synthesis

Preparation of the UVM-7 support was synthesized by a method based on the atrane route,[82] with a molar composition of $2Si(OC_2H_5)_4$:$7(HOCH_2CH_2)_3N.HCl$:$0.52CH_3(CH_2)_{15}N(Br)(CH_3)_3$:$180H_2O$. In a standard synthesis, corresponding amounts of $Si(OC_2H_5)_4$ and $(HOCH_2CH_2)_3N.HCl$ were mixed under continuous stirring at 140 °C, forming a homogeneous dispersion. The temperature was then set to 120 °C and $CH_3(CH_2)_{15}N(Br)(CH_3)_3$ was incorporated. The resulting gel was then cooled to 80 °C, followed by the addition of deionized water. The mixture was stirred and aged at room temperature for 16 h. The mesostructured powder was separated by filtration and washed extensively with deionized water and ethanol. Finally, the powder was dried for 16 h at 60 °C. To prepare the final porous material, the template was removed by calcination at 550 °C for 6 h under static air, with a ramp rate of 5 °C min^{-1} from ambient.

Preparation of the 40 wt% ZrO_2/UVM-7 support was achieved using a wet impregnation method. $ZrO(NO_3)_2.xH_2O$ (1.48 g) was dissolved in 30 mL of deionized water under vigorous stirring. The UVM-7 material (0.6 g) was added to the nitrate solution, followed by stirring the sample for 13 h. The mixture was then dried overnight at 110 °C, and the resulting material was calcined in air at 550 °C for 4 h, with a ramp rate of 1 °C min^{-1} from ambient.

A 40 wt% ZrO_2/UVM-7 support was selected as previous work showed poor catalytic activity for Au-Pt based catalysts deposited on pure ZrO_2 and pure siliceous UVM-7 compared with ZrO_2/UVM-7. Different ZrO_2 loadings were tested and found that 40 wt% ZrO_2 was optimal. A comparison of metal oxide supports was also carried out and found the ZrO_2 was the most active support. Examples of these preliminary tests are shown as Supporting Information (Figures S1 and S2).

Mono- and bimetallic Pt/Au-supported catalysts were synthesized by a colloidal deposition method. To synthesize the Au/Pt colloids, fresh aqueous solutions of $(HOCH_2)_4PCl$ (0.0675 M) and NaOH (0.2 M) were prepared by adding 1.5 mL of NaOH and 1 mL of $(HOCH_2)_4PCl$ to 45.5 mL of deionized water. An appropriate amount of aqueous Au or Pt precursor solution ($KAuCl_4$ or $PtCl_4$) was then added under vigorous stirring at 60 °C. The hydrosols were stirred for 30 min, followed by the addition of the desired amount of 40 wt% ZrO_2/UVM-7 (acidified to pH 2 by H_2SO_4) to obtain the required metal loading. The slurry was stirred for 2 h, collected by filtration, and then washed thoroughly with deionized water and dried at 120 °C for 16 h in static air. The final material was calcined in air at 400 °C for 2 h, heating from ambient with a ramp rate of 5 °C min^{-1}. For the bimetallic catalysts, the required amounts of aqueous $KAuCl_4$/$PtCl_4$ solutions were added simultaneously. However, for the catalysts prepared by different orders of loading, the aqueous $KAuCl_4$/$PtCl_4$ solutions were added consecutively with the drying and calcination processes occurring between each metal loading.

4.2. Catalyst Characterization

Powder X-ray diffraction (XRD) was performed using a Panalytical X'Pert diffractometer, equipped with a Cu X-ray source. Operating conditions for the diffractometer were 40 kV and 40 mA, with analysis carried out between 2θ values of 5°–80°. Phase identification was performed by matching patterns against the ICDD standard database. Application of the Scherrer equation was used to estimate crystallite size.

Temperature programmed reduction (TPR) was performed using a Quantachrome ChemBET. Catalysts underwent pre-treatment for 1 h at 120 °C in a flow of He before analysis. Reduction profiles were obtained by analyzing powdered catalysts (50 mg) under a flow of 10% H_2/Ar (50 mL min^{-1}), over the temperature range 50–700 °C, with a heating rate of 10 °C min^{-1}. H_2 consumption was calculated by calibration against a CuO standard.

X-ray photoelectron spectroscopy (XPS) was performed on a Thermo Fisher Scientific K-alpha+ spectrometer. Samples were analyzed using a micro-focused monochromatic Al x-ray source (72 W) using the "400-micron spot" mode, which provides an analysis defining an elliptical x-ray spot of ca. 400 × 600 microns. Data was recorded at pass energies of 150 eV for survey scans and 50 eV for high-resolution scans with step sizes of 1 and 0.1 eV, respectively; the dwell time was 50 and 10 ms in each case. As the samples were insulating, charge compensation was achieved using a combination of both low-energy electrons and argon ions.

Data analysis was performed in CasaXPS v2.3.26[83] after calibrating the data to the lowest C (1s) component taken to have a value of 284.8 eV. Quantification was made using a Shirley-type background and Scofield cross sections, with an electron energy dependence based on the TPP-2M relationship.[84] Peak fitting was performed using the CasaXPS LA line shape, which is Voigt-like. All parameters for LA shape were derived from standard reference materials where possible.

CO-Diffuse reflectance infrared Fourier transformed spectroscopy (DRIFTS) measurements were obtained using a Bruker Tensor 27 spectrometer, fitted with a Hg-Cd-Te detector and ZnSe windows. Powder samples were loaded into the Praying Mantis high-temperature (HVC-DRP-4) in situ cell, followed by a pre-treatment with flowing N_2 (50 mL min^{-1}). A background was obtained using KBr, and measurements were recorded every minute at room temperature. 1% CO/N_2 was flowed over the sample at 50 mL min^{-1} until CO adsorption bands were maintained constant. Once CO bands were constant, the gas feed was changed to purge with N_2, and measurements were made until no change in subsequent spectra was observed.

Electron microscopy analyses were carried out in a FEI XFEG Titan transmission electron microscope operated at 300 kV. The column was fitted with a CEOS spherical aberration corrector (Cs-corrected) for the electron probe, assuring a spatial resolution of 0.8 Å (prior to each analysis, the aberrations were reduced to a gold standard sample). The microscope was also equipped with an Oxford Ultim X-MaxN 100TLE X-EDS detector and a Gatan Tridiem Energy Filter (GIF) for electron energy loss spectroscopic (EELS) measurements. The samples were prepared by dispersing a small amount of the powder in ethanol; a few drops of the suspension were placed onto holey carbon grids. All measurements were performed in scanning mode (STEM) using a high-angle annular dark field detector (HAADF).

4.3. Catalyst Testing

The simultaneous total oxidation of propene, toluene, and CO was performed using a fixed bed flow microreactor. Powder catalysts

© 2025 The Author(s). ChemCatChem published by Wiley-VCH GmbH

18673899, 0, Downloaded from https://chemistry-europe.onlinelibrary.wiley.com/doi/10.1002/cctc.202401462 by Welsh Assembly Government, Wiley Online Library on [13/03/2025]. See the Terms and Conditions (https://onlinelibrary.wiley.com/terms-and-conditions) on Wiley Online Library for rules of use; OA articles are governed by the applicable Creative Commons License

18673899, 0, Downloaded from https://chemistry-europe.onlinelibrary.wiley.com/doi/10.1002/cctc.202401462 by Welsh Assembly Government, Wiley Online Library on [13/03/2025]. See the Terms and Conditions (https://onlinelibrary.wiley.com/terms-and-conditions) on Wiley Online Library for rules of use; OA articles are governed by the applicable Creative Commons License

(50 mg) were packed between plugs of quartz wool in a $\frac{1}{2}$ inch quartz tube. Catalysts were pre-treated for 1 h at 100 °C, under a flow of N_2 at 50 mL min^{-1}. Following pre-treatment, the reaction mixture of 1000 ppm propene, 1000 ppm CO, and 100 ppm toluene in 6% O_2 with N_2 balance was passed through the bypass loop until stabilized to acquire a background measurement. The reaction gas mixture was then passed through the catalyst bed at 50 mL min^{-1} to achieve a WHSV of 60,000 mL g^{-1} h^{-1}. Catalyst activity was measured over the temperature range of 100–500 °C at 50 °C intervals (allowing time to reach steady state), with a K-type thermocouple placed in the catalyst bed to monitor the reaction temperature. The effluent analysis was recorded by a quantitative on-line Gasmet DX-4000 FT-IR process spectrometer, with measurements taken every second. Calcmet software was used to convert measured the response to quantitative concentrations using a library of calibration files. An average of 10 measurements was recorded at each temperature interval once steady state had been achieved. CO_2 yield was used to define the conversion of propene, toluene, and CO to CO_2. The recorded concentration of CO_2 was compared to the sum of all compound concentrations, using carbon equivalents. Catalyst testing errors were calculated using the standard deviation when testing a standard catalyst three times under the stated reaction conditions. For CO_2 yield, the error was ±3%.

Acknowledgements

A.M., M.P.F., and R.A. acknowledge the Spanish MICIU for funding (CEX2023-001286-S MICIU/AEI /10.13039/501100011033) as well as the regional government of Aragon (DGA E13_23R). The microscopy works have been conducted in the Laboratorio de Microscopias Avanzadas (LMA) at the Universidad de Zaragoza. R.A. and A.M. also acknowledge the support of the Spanish MICIU (PID2023-151080NB-I00/AEI/10.13039/501100011033 and CNS2023-144346-AEI /10.13039/501100011033, respectively). M.P.F. acknowledges the support of the Spanish MICIU (Ayudas Margarita Salas). B.S. thanks the MCIN/AEI through the project TED2021-129555B-I00/ AEI/10.13039/501100011033/ Unión Europea NextGeneration EU/PRTR. P.A. thanks PID2021-126304OB-C43 funded by MCIN/AEI/ 10.13039/501100011033 and by "ERDF A way of making Europe." T.G. would like to acknowledge the Spanish Ministry of Science, Innovation and Universities through its Mobility program for stays of senior researchers and professors in foreign countries (PRX18/00474) and the regional government of Aragon (DGA T04_20R) for funding. XPS analysis work was performed through the support of the EPSRC National Facility for X-ray photoelectron spectroscopy ('HarwellXPS', Grant numbers EP/Y023587/1, EP/Y023609/1, EP/Y023536/1, EP/Y023552/1, and EP/Y023544/1).

Conflict of Interests

The authors declare no conflict of interest.

Data Availability Statement

The data that support the findings of this study are available from the corresponding author upon reasonable request. The XPS data that support the findings of this study are openly available at http://doi.org/10.17035/cardiff.28344143.

Keywords: Environmental chemistry · Gas-phase reactions · Heterogeneous catalysis · Nanoparticles · Oxidation

[1] Z. H. Ling, H. Guo, *Environ. Sci. Policy* **2014**, *38*, 180–191.
[2] P. Jookjantra, S. Thepanondh, J. Keawboonchu, V. Kultan, W. Laowagul, *J. Environ. Qual.* **2022**, *51*, 1016–1034.
[3] D. J. Wuebbles, S. Sanyal, *Curr. Pollut. Rep.* **2015**, *1*, 117–129.
[4] A. Ragothaman, W. A. Anderson, *Environments* **2017**, *4*, 66.
[5] M. S. Reiter, K. M. Kockelman, *Transp. Res. Part Transp. Environ.* **2016**, *43*, 123–132.
[6] L. Fang, D. Lou, Z. Hu, P. Tan, *Energies* **2019**, *12*, 3556.
[7] Z. Zhang, H. Man, J. Zhao, Y. Jiang, M. Zeng, Z. Cai, C. Huang, W. Huang, H. Zhao, S. Jing, X. Shi, K. He, H. Liu, *J. Hazard. Mater.* **2022**, *435*, 128979.
[8] M. Ousmane, L. F. Liotta, G. D. Carlo, G. Pantaleo, A. M. Venezia, G. Deganello, L. Retailleau, A. Boreave, A. Giroir-Fendler, *Appl. Catal. B Environ.* **2011**, *101*, 629–637.
[9] F. Pariselli, M. G. Sacco, J. Ponti, D. Rembges, *Exp. Toxicol. Pathol.* **2009**, *61*, 381–386.
[10] J.-O. Jo, H. Q. Trinh, S. H. Kim, Y. S. Mok, *Chem. Eng. J.* **2016**, *299*, 93–103.
[11] A. L. Chiew, N. A. Buckley, *Crit. Care* **2014**, *18*, 221.
[12] G. R. Parmar, N. N. Rao, *Crit. Rev. Environ. Sci. Technol.* **2008**, *39*, 41–78.
[13] A. Krishnamurthy, B. Adebayo, T. Gelles, A. Rownaghi, F. Rezaei, *Catal. Today* **2020**, *350*, 100–119.
[14] S. Scirè, L. F. Liotta, *Appl. Catal. B Environ.* **2012**, *125*, 222–246.
[15] A. C. Gluhoi, N. Bogdanchikova, B. E. Nieuwenhuys, *J. Catal.* **2005**, *229*, 154–162.
[16] P. Gélin, M. Primet, *Appl. Catal. B Environ.* **2002**, *39*, 1–37.
[17] T. Barakat, V. Idakiev, R. Cousin, G.-S. Shao, Z.-Y. Yuan, T. Tabakova, S. Siffert, *Appl. Catal. B* **2014**, *146*, 138–146.
[18] S. Huang, C. Zhang, H. He, *Catal. Today* **2008**, *139*, 15–23.
[19] V. P. Santos, S. A. C. Carabineiro, P. B. Tavares, M. F. R. Pereira, J. J. M. Órfão, J. L. Figueiredo, *Appl. Catal. B Environ.* **2010**, *99*, 198–205.
[20] L. F. Liotta, *Appl. Catal. B Environ.* **2010**, *100*, 403–412.
[21] A. C. Gluhoi, N. Bogdanchikova, B. E. Nieuwenhuys, *Catal. Today* **2006**, *113*, 178–181.
[22] K. M. Saoud, M. S. El-Shall, *Catalysts* **2020**, *10*, 1351.
[23] M. Hosseini, T. Barakat, R. Cousin, A. Aboukaïs, B.-L. Su, G. De Weireld, S. Siffert, *Appl. Catal. B Environ.* **2012**, *111–112*, 218–224.
[24] R. Fiorenza, *Catalysts* **2020**, *10*, 661.
[25] T. K. Nevanperä, S. Ojala, T. Laitinen, S. Pitkäaho, S. Saukko, R. L. Keiski, *Catalysts* **2019**, *9*, 603.
[26] K.-J. Kim, H.-G. Ahn, *Appl. Catal. B Environ.* **2009**, *91*, 308–318.
[27] A. Villa, D. Wang, D. S. Su, L. Prati, *Catal. Sci. Technol.* **2014**, *5*, 55–68.
[28] T. Barakat, J. C. Rooke, D. Chlala, R. Cousin, J.-F. Lamonier, J.-M. Giraudon, S. Casale, P. Massiani, B.-L. Su, S. Siffert, *Catalysts* **2018**, *8*, 574.
[29] X. Fu, Y. Liu, W. Yao, Z. Wu, *Catal. Commun.* **2016**, *83*, 22–26.
[30] B. Solsona, M. Pérez-Cabero, I. Vázquez, A. Dejoz, T. García, J. Álvarez-Rodríguez, J. El-Haskouri, D. Beltrán, P. Amorós, *Chem. Eng. J.* **2012**, *187*, 391–400.
[31] M. M. Trandafir, A. Moragues, P. Amorós, V. I. Parvulescu, *Catal. Today* **2020**, *355*, 893–902.
[32] M. Pérez-Cabero, J. E. Haskouri, B. Solsona, I. Vázquez, A. Dejoz, T. García, J. Álvarez-Rodríguez, A. Beltrán, D. Beltrán, P. Amorós, *J. Mater. Chem.* **2010**, *20*, 6780–6788.
[33] A. Moragues, B. Puértolas, Á. Mayoral, R. Arenal, A. B. Hungría, S. Murcia-Mascarós, S. H. Taylor, B. Solsona, T. García, P. Amorós, *J. Catal.* **2018**, *360*, 187–200.
[34] P. Peng, J. Li, S. Mo, Q. Zhang, T. Shen, Q. Xie, *Processes* **2021**, *9*, 230.
[35] R. K. Dadi, D. Luss, V. Balakotaiah, *Chem. Eng. J.* **2016**, *304*, 941–952.
[36] Q. Zhang, S. Mo, J. Li, Y. Sun, M. Zhang, P. Chen, M. Fu, J. Wu, L. Chen, D. Ye, *Catal. Sci. Technol.* **2019**, *9*, 4538–4551.
[37] C. Colbea, D. Avram, B. Cojocaru, R. Negrea, C. Ghica, V. G. Kessler, G. A. Seisenbaeva, V. Parvulescu, C. Tiseanu, *Nanomaterials* **2018**, *8*, 988.
[38] L.-H. Chang, N. Sasirekha, Y.-W. Chen, W.-J. Wang, *Ind. Eng. Chem. Res.* **2006**, *45*, 4927–4935.

© 2025 The Author(s). ChemCatChem published by Wiley-VCH GmbH

[39] Z. Tang, P. Liu, H. Cao, S. Bals, H. J. Heeres, P. P. Pescarmona, *ACS Catal.* **2019**, *9*, 9953–9963.
[40] Y. Liu, H. Dai, J. Deng, S. Xie, H. Yang, W. Tan, W. Han, Y. Jiang, G. Guo, *J. Catal.* **2014**, *309*, 408–418.
[41] Z. Han, L. Dai, Y. Liu, J. Deng, L. Jing, Y. Zhang, K. Zhang, X. Zhang, Z. Hou, W. Pei, H. Dai, *Catal. Today* **2021**, *376*, 134–143.
[42] H. Yang, J. Deng, Y. Liu, S. Xie, Z. Wu, H. Dai, *J. Mol. Catal. Chem.* **2016**, *414*, 9–18.
[43] S. Oh, S. Back, W. H. Doh, S. Y. Moon, J. Kim, Y. Jung, J. Y. Park, *RSC Adv.* **2017**, *7*, 45003–45009.
[44] K. Balakrishnan, J. Schwank, *J. Catal.* **1992**, *138*, 491–499.
[45] M. Haruta, M. Daté, *Appl. Catal. Gen.* **2001**, *222*, 427–437.
[46] E. A. Redina, O. A. Kirichenko, A. A. Greish, A. V. Kucherov, O. P. Tkachenko, G. I. Kapustin, I. V. Mishin, L. M. Kustov, *Catal. Today* **2015**, *246*, 216–231.
[47] N. F. P. Ribeiro, F. M. T. Mendes, C. A. C. Perez, M. M. V. M. Souza, M. Schmal, *Appl. Catal. Gen.* **2008**, *347*, 62–71.
[48] B. Koslowski, H.-G. Boyen, C. Wilderotter, G. Kästle, P. Ziemann, R. Wahrenberg, P. Oelhafen, *Surf. Sci.* **2001**, *475*, 1–10.
[49] S. Zhou, G. S. Jackson, B. Eichhorn, *Adv. Funct. Mater.* **2007**, *17*, 3099–3104.
[50] J. H. Carter, X. Liu, Q. He, S. Althahban, E. Nowicka, S. J. Freakley, L. Niu, D. J. Morgan, Y. Li, J. W. (Hans) Niemantsverdriet, S. Golunski, C. J. Kiely, G. J. Hutchings, *Angew. Chem., Int. Ed.* **2017**, *56*, 16037–16041.
[51] A. S. Aricò, A. K. Shukla, H. Kim, S. Park, M. Min, V. Antonucci, *Appl. Surf. Sci.* **2001**, *172*, 33–40.
[52] S. Viéitez-Calo, D. J. Morgan, S. Golunski, S. H. Taylor, M. V. Twigg, *Top. Catal.* **2021**, *64*, 955–964.
[53] R. P. Doherty, J.-M. Krafft, C. Méthivier, S. Casale, H. Remita, C. Louis, C. Thomas, *J. Catal.* **2012**, *287*, 102–113.
[54] Y. Xu, Y. Dong, J. Shi, M. Xu, Z. Zhang, X. Yang, *Catal. Commun.* **2011**, *13*, 54–58.
[55] T. Garcia, S. Agouram, S. H. Taylor, D. Morgan, A. Dejoz, I. Vázquez, B. Solsona, *Catal. Today* **2015**, *254*, 12–20.
[56] F. Schüth, *Phys. Status Solidi B* **2013**, *250*, 1142–1151.
[57] M.-Y. Kim, J.-S. Choi, T. J. Toops, E.-S. Jeong, S.-W. Han, V. Schwartz, J. Chen, *Catalysts* **2013**, *3*, 88–103.
[58] K.-J. Kim, S.-I. Boo, H.-G. Ahn, *J. Ind. Eng. Chem.* **2009**, *15*, 92–97.
[59] H. Qin, X. Qian, T. Meng, Y. Lin, Z. Ma, *Catalysts* **2015**, *5*, 606–633.
[60] S. K. Jain, E. M. Crabb, L. E. Smart, D. Thompsett, A. M. Steele, *Appl. Catal. B Environ.* **2009**, *89*, 349–355.
[61] L. Ilieva, A. M. Venezia, P. Petrova, G. Pantaleo, L. F. Liotta, R. Zanella, Z. Kaszkur, T. Tabakova, *Catalysts* **2018**, *8*, 283.
[62] T. Tabakova, L. Ilieva, P. Petrova, A. M. Venezia, Y. Karakirova, L. F. Liotta, G. Avdeev, *Appl. Sci.* **2020**, *10*, 1088.
[63] S. W. Chee, J. M. Arce-Ramos, W. Li, A. Genest, U. Mirsaidov, *Nat. Commun.* **2020**, *11*, 2133.
[64] Y.-F. Y. Yao, *J. Catal.* **1984**, *87*, 152–162.
[65] D. Chlala, M. Labaki, J.-M. Giraudon, O. Gardoll, A. Denicourt-Nowicki, A. Roucoux, J.-F. Lamonier, *Comptes Rendus Chim* **2016**, *19*, 525–537.
[66] M. Haruta, S. Tsubota, T. Kobayashi, H. Kageyama, M. J. Genet, B. Delmon, *J. Catal.* **1993**, *144*, 175–192.
[67] H. Ha, H. An, M. Yoo, J. Lee, H. Y. Kim, *J. Phys. Chem. C* **2017**, *121*, 26895–26902.
[68] A. Buzková Arvajová, J. Březina, R. Pečinka, P. Kočí, *Appl. Catal. B Environ.* **2018**, *233*, 167–174.
[69] A.-C. Yang, V. Streibel, T. S. Choksi, H. Aljama, B. Werghi, S. R. Bare, R. S. Sánchez-Carrera, A. Schäfer, Y. Li, F. Abild-Pedersen, M. Cargnello, *J. Catal.* **2021**, *401*, 89–101.
[70] A. Aznárez, A. Gil, S. A. Korili, *RSC Adv.* **2015**, *5*, 82296–82309.
[71] N. Radic, B. Grbic, A. Terlecki-Baricevic, *Appl. Catal. B Environ.* **2004**, *50*, 153–159.
[72] L. Lu, Y. Nie, Y. Wang, G. Wu, L. Li, J. Li, X. Qi, Z. Wei, *J. Mater. Chem. A* **2018**, *6*, 104–109.
[73] S. Eaimsumang, N. Chollacoop, A. Luengnaruemitchai, S. H. Taylor, *Front. Chem.* **2022**, *10*.
[74] E. Genty, J. Brunet, C. Poupin, S. Ojala, S. Siffert, R. Cousin, *Appl. Catal. B Environ.* **2019**, *247*, 163–172.
[75] M. Piumetti, D. Fino, N. Russo, *Appl. Catal. B Environ.* **2015**, *163*, 277–287.
[76] E. Sartoretti, F. Martini, M. Piumetti, S. Bensaid, N. Russo, D. Fino, *Catalysts* **2020**, *10*, 165.
[77] G. Rochard, L. Olivet, M. Tannous, C. Poupin, S. Siffert, R. Cousin, *Catalysts* **2021**, *11*, 1218.
[78] S. M. Saqer, D. I. Kondarides, X. E. Verykios, *Top. Catal.* **2009**, *52*, 517–527.
[79] Y. Shen, J. Deng, X. Hu, X. Chen, H. Yang, D. Cheng, D. Zhang, *Environ. Sci. Technol.* **2023**, *57*, 1797–1806.
[80] S. Ali, L. Chen, F. Yuan, R. Li, T. Zhang, S. I. H. Bakhtiar, X. Leng, X. Niu, Y. Zhu, *Appl. Catal. B Environ.* **2017**, *210*, 223–234.
[81] B. Puértolas, Á. Mayoral, R. Arenal, B. Solsona, A. Moragues, S. Murcia-Mascaros, P. Amorós, A. B. Hungría, S. H. Taylor, T. García, *ACS Catal.* **2015**, *5*, 1078–1086.
[82] M. Pérez-Cabero, A. B. Hungría, J. M. Morales, M. Tortajada, D. Ramón, A. Moragues, J. E. Haskouri, A. Beltrán, D. Beltrán, P. Amorós, *J. Nanoparticle Res.* **2012**, *14*, 1045.
[83] N. Fairley, V. Fernandez, M. Richard-Plouet, C. Guillot-Deudon, J. Walton, E. Smith, D. Flahaut, M. Greiner, M. Biesinger, S. Tougaard, D. Morgan, J. Baltrusaitis, *Appl. Surf. Sci. Adv.* **2021**, *5*, 100112.
[84] S. Tanuma, C. J. Powell, D. R. Penn, *Surf. Interface Anal.* **2003**, *35*, 268–275.

Manuscript received: August 24, 2024
Revised manuscript received: January 23, 2025
Accepted manuscript online: January 30, 2025
Version of record online: ■■, ■■

© 2025 The Author(s). ChemCatChem published by Wiley-VCH GmbH

18673899, 0, Downloaded from https://chemistry-europe.onlinelibrary.wiley.com/doi/10.1002/cctc.202401462 by Welsh Assembly Government, Wiley Online Library on [13/03/2025]. See the Terms and Conditions (https://onlinelibrary.wiley.com/terms-and-conditions) on Wiley Online Library for rules of use; OA articles are governed by the applicable Creative Commons License